AFRL-AFOSR-VA-TR-2020-0081

Exploiting the Non-linear Interactions within Wall Turbulence for Flow Control

Ebenezer Gnanamanickam
EMBRY-RIDDLE AERONAUTICAL UNIVERSITY

03/30/2020
Final Report

Air Force Research Laboratory
AF Office Of Scientific Research (AFOSR)/ RTA1
Arlington, Virginia 22203
Air Force Materiel Command

REPORT DOCUMENTATION PAGE

Form Approved
OMB No. 0704-0188

1. REPORT DATE *(DD-MM-YYYY)*	2. REPORT TYPE	3. DATES COVERED *(From - To)*
30-06-2020	Final Performance	01 Jul 2016 to 31 Dec 2019

4. TITLE AND SUBTITLE
Exploiting the Non-linear Interactions within Wall Turbulence for Flow Control

5a. CONTRACT NUMBER

5b. GRANT NUMBER
FA9550-16-1-0194

5c. PROGRAM ELEMENT NUMBER
61102F

6. AUTHOR(S)
Ebenezer Gnanamanickam

5d. PROJECT NUMBER

5e. TASK NUMBER

5f. WORK UNIT NUMBER

7. PERFORMING ORGANIZATION NAME(S) AND ADDRESS(ES)
EMBRY-RIDDLE AERONAUTICAL UNIVERSITY
600 S CLYDE MORRIS BLVD
DAYTONA BEACH, FL 32114 US

8. PERFORMING ORGANIZATION REPORT NUMBER

9. SPONSORING/MONITORING AGENCY NAME(S) AND ADDRESS(ES)
AF Office of Scientific Research
875 N. Randolph St. Room 3112
Arlington, VA 22203

10. SPONSOR/MONITOR'S ACRONYM(S)
AFRL/AFOSR RTA1

11. SPONSOR/MONITOR'S REPORT NUMBER(S)
AFRL-AFOSR-VA-TR-2020-0081

12. DISTRIBUTION/AVAILABILITY STATEMENT
A DISTRIBUTION UNLIMITED: PB Public Release

13. SUPPLEMENTARY NOTES

14. ABSTRACT
The flow interactions and mechanism within complex wall-bounded flows were studied using the plane wall jet (PWJ) as the model flow field. The PWJ is forced using large-amplitude, large-scale, acoustic forcing. In this manner a controlled flow scale is introduced into the base flow and the resulting flow mechanism are studied. Complimentary hot-wire anemometry and particle image velocimetry measurements were carried out on a forced and unforced PWJ. A range of forcing scales were studied and all the forcing scales resulted in a reduction in friction velocity at all streamwise locations considered. Three different flow scales were chosen to examine in detail the energy transfer mechanisms within the forced PWJ. The forcing resulted in a large increase in the streamwise turbulence intensity in the wall region, specifically in the large-scale intensities. The linear response of the PWJ resulted in flow structures that resembled the naturally occurring flow structures in the unforced flow. These are the boundary layer like structures in the wall region and jet like structures in the outer free shear layer. The excess energy from forcing was transferred to scales of the wavelength of the outer jet like structures, though this occurred in the wall region. This energy transfer occurred irrespective of the direction of the transfer. At the upstream locations, the direction if energy transfer was in the manner of a forward cascade while at the downstream locations it was in the manner of an inverse cascade. It was then concluded that the natural energy transfer pathway in the PWJ was to transfer energy away from the wall region structures into the outer jet like structures. The forcing then isolates a single energy transfer pathway where the input energy is at the forcing scales. These observations lends support to the viewpoint that the linear dynamics of the Navier-Stokes eq

15. SUBJECT TERMS
wall plane jet, large and small scale interactions

16. SECURITY CLASSIFICATION OF:			17. LIMITATION OF ABSTRACT	18. NUMBER OF PAGES	19a. NAME OF RESPONSIBLE PERSON
a. REPORT	b. ABSTRACT	c. THIS PAGE			ABATE, GREGG
Unclassified	Unclassified	Unclassified	UU		19b. TELEPHONE NUMBER *(Include area code)* 703-588-1779

(YIP) Exploiting the non-linear interactions within wall turbulence for flow control

Ebenezer P. Gnanamanickam

Doctoral students - Shibani Bhatt & Artham Sravan Kumar

Embry-Riddle Aeronautical University, Daytona Beach, FL, 32119

Abstract

The flow interactions and mechanism within complex wall-bounded flows were studied using the plane wall jet (PWJ) as the model flow field. The PWJ is forced using large-amplitude, large-scale, acoustic forcing. In this manner a controlled flow scale is introduced into the base flow and the resulting flow mechanism are studied. Complimentary hot-wire anemometry and particle image velocimetry measurements were carried out on a forced and unforced PWJ. A range of forcing scales were studied and all the forcing scales resulted in a reduction in friction velocity at all streamwise locations considered. Three different flow scales were chosen to examine in detail the energy transfer mechanisms within the forced PWJ. The forcing resulted in a large increase in the streamwise turbulence intensity in the wall region, specifically in the large-scale intensities. The linear response of the PWJ resulted in flow structures that resembled the naturally occurring flow structures in the unforced flow. These are the boundary layer like structures in the wall region and jet like structures in the outer free shear layer. The excess energy from forcing was transferred to scales of the wavelength of the outer jet like structures, though this occurred in the wall region. This energy transfer occurred irrespective of the direction of the transfer. At the upstream locations, the direction if energy transfer was in the manner of a forward cascade while at the downstream locations it was in the manner of an inverse cascade. It was then concluded that the natural energy

transfer pathway in the PWJ was to transfer energy away from the wall region structures into the outer jet like structures. The forcing then isolates a single energy transfer pathway where the input energy is at the forcing scales. These observations lends support to the viewpoint that the linear dynamics of the Navier-Stokes equations dictate the nature of the large-scale structures in the flow. The flow non-linearities then redistribute the energy between flow scales. However as highlighted in this work this transfer can be either in the manner of a forward cascade or an inverse cascade. The inner-outer interaction was also found to be enhanced by the forcing thus establishing a viable means to control these flows using large-scale inputs.

1. Introduction

It has recently been observed that the large-scale motions within turbulent boundary layers interact with the smaller scales in the flow, in a non-linear manner, through a process of amplitude and frequency modulation [1–6]. Here the term large-scale refers to flow structures larger than the some outer length scale such as the boundary layer thickness. The long term goal of this work is to control wall turbulence by exploiting this non-linear interaction through large-scale inputs to the flow. The large-scale motions within wall turbulence are attractive targets for active flow control as the scale size of devices and sensors required are much more feasible from an engineering perspective. The required frequency response of such sensors and actuators are fairly low (a few 100 Hz). The larger scales are also the dominant energy carrying eddies at high Reynolds numbers and persist for long distances (or time periods), thereby increasing the effective region under control [4]. These practical considerations along with the recent advances in understanding the interactions between the large-scale and small-scales within a boundary layer, makes targeting the large-scales of wall turbulence an attractive proposition.

The modulation effect of the large-scale on the smaller scales were initially observed by Brown and Thomas [7] and then by Bandyopadhyay and Hussain [8]. However, after receiving very little attention for almost two decades, several recent studies have focused on the interaction between the large-scale and small-scale motions within a boundary layer, particularly with increasing Reynolds number [1–3, 5, 9–16]. It has been established that the large-scales linearly superimpose themselves on the small-scales while also having a non-linear, amplitude and frequency modulation effect on the small-scales.

The principal investigator (PI) carried out a fundamental study characterizing this non-linear interaction through systematic perturbation of the large-scales. The model boundary layer chosen for this work is the the plane wall jet (PWJ). A PWJ is a two-dimensional jet

that exits tangentially along a flat plate into either quiescent fluid or a fluid stream (co-flow) [17, 18] – see schematic of Fig. 1. The PWJ considered was primarily into quiescent air. However, in the final year of performance a new PWJ facility with a co-flow was built and the resulting flow was studied. A PWJ has two shear layers that transition to turbulence through different mechanisms. On one hand, the outer free-shear layer (free jet portion), transitions via an inviscid mechanism (Kelvin-Helmholtz instability), naturally leading to energetic large-scales. On the other hand, the inner shear layer (boundary layer portion) transitions through a viscous mechanism, which leads to finer scales of turbulence. These shear layers then interact as the flow develops downstream of the exit.

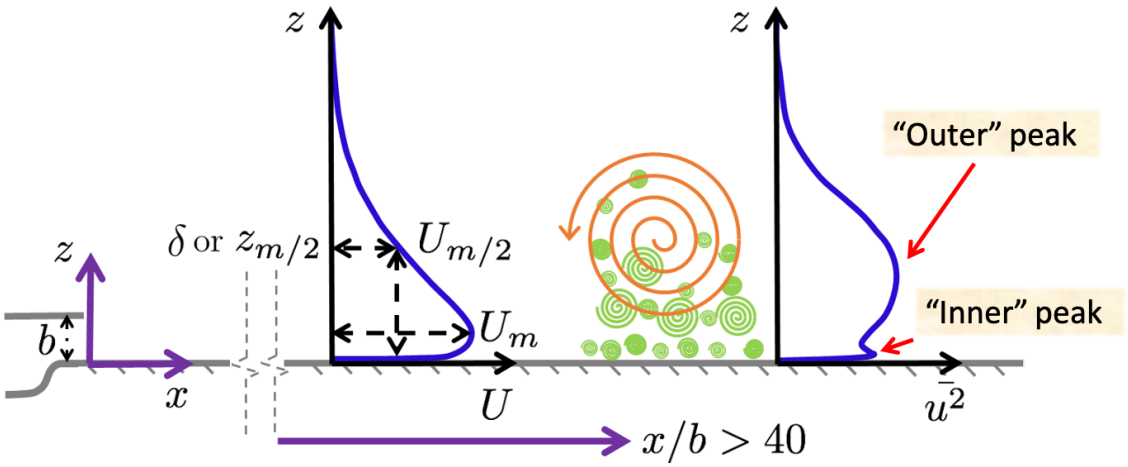

Figure 1: Schematic of a PWJ shear layer. Here, x and z denote streamwise and wall-normal directions respectively, b the jet exit height, U the mean streamwise velocity and u the velocity fluctuation.

The PWJ reaches a self-preserving state at distances greater than $x/b > 40$ where x is the stream-wise direction and b the PWJ exit height (Fig. 1). A schematic of the mean stream-wise velocity profile U is shown in Fig. 1; the mean velocity has been non-dimensionalized using the maximum velocity U_m, which is the outer velocity scale. The outer length scale δ is the wall normal distance where the streamwise velocity is $U_m/2$, as shown in Fig. 1. Also shown is a schematic of the non-dimensionalized streamwise turbulence intensity pro-

file. Seen clearly are two peaks, i.e. an outer larger peak corresponding to the energetic large outer scales and an inner smaller peak associated with the near-wall turbulence cycle as seen in canonical boundary layers (e.g., zero-pressure gradient, pipe flow).

The PWJ is chosen as the model flow field primarily for this reason – a natural separation of scales exists as the turbulence arises from two distinct sources. Furthermore, the outer larger scales in a PWJ are extremely energetic, large-scales with inner-scaled energy density comparable to that seen in very high Reynolds numbers. The inherent configuration of the PWJ also allows for the control (or perturbation) of the outer larger scales independent of the inner cycle, particularly in a flow regime where the large-scales are extremely energetic. On the other hand, the inner-cycle develops with energy density comparable to canonical boundary layers which allows the use of the PWJ to study the effect of large-scale perturbations.

Studies have been carried out where the energetic large outer scales of the PWJ were modified [19–21]. Schober and Femholz [21] conducted experiments on a PWJ in which the outer shear layer structures were excited using an oscillating wire and also suppressed using a still wire. On the one hand, Schober and Femholz [21] and Zhou et al. [20] (Zhou et al. [20] used acoustic excitation) found that the excitation increased the coherence of the large-scales, which resulted in an increase in turbulence intensity of the streamwise velocity fluctuations. On the other hand, Schober and Femholz [21] showed that suppressing turbulence had the opposite effect. Schober and Femholz [21] also observed that there was a reduction in the mean (time-averaged) skin friction at the wall when the jet was excited; conversely there was an increase in skin friction when the turbulence was suppressed. Katz et al. [19] also reported a reduction in skin friction to various degrees based on the forcing frequency. These prior studies serve as a motivation for the present work. As part of the present work, it is sought to describe the internal mechanisms within a forced PWJ that lead to these changes in the near-wall region due to large-scale forcing. Lessons are also sought to be learnt that

can aid in modelling and controlling complex wall-bounded flows a large.

Relevance to the Air Force - Apart from the basic physics benefit of understanding interactions within complex wall-bounded flows, the PWJ has other direct benefits to the Air Force. Due to the large-scale mixing present in the PWJ, the PWJ has been used as the prototypical model flow field to study mixing and reactions [22–24]. Controlling the energetic, large-scales in the flow has direct relevance to controlling reaction and mixing rates in reacting systems. The nature of the interaction between the outer large-scales and the inner small-scales in a PWJ also has some similarities with the post-reattachment region of near-wall shear layers [25] and jet impingements (seen in heating/cooling applications as well as in Vertical Take Off and Landing vehicles/rotorcraft in ground effect [26–30]). PWJ type flows are also encountered both in the boundary layer development of multi-element airfoils and more prominently in film cooling of turbine blades and combustion chambers [18, 31]. In film cooling, the large-scales are the scales that are responsible for either enhanced or suppressed mixing of the cooling layer, with the surrounding combustion gases. The control of the large-scales in these flows offers the possibility of actively controlling the mixing between the layers. Thus the basic physics goals of this proposed work has relevance and significance to a wide variety of flow fields that are of interest to the Air Force, apart from the inherent insight obtained into complex wall-bounded flow in general.

2. Experimental Approach

Measurements were primarily carried out in a PWJ facility a schematic of which is shown in figure 2. Air from a centrifugal fan passed through a series of screens and entered a plenum settling chamber. The air then passed through a honeycomb layer and into a two-dimensional contraction of ratio 16:1. The exit of the rectangular nozzle had a width $b =$ 5 mm with an aspect ratio of 128. A strip of sand paper was installed across the facility floor, past the nozzle exit, which trips the boundary layer. This trip was used to minimize,

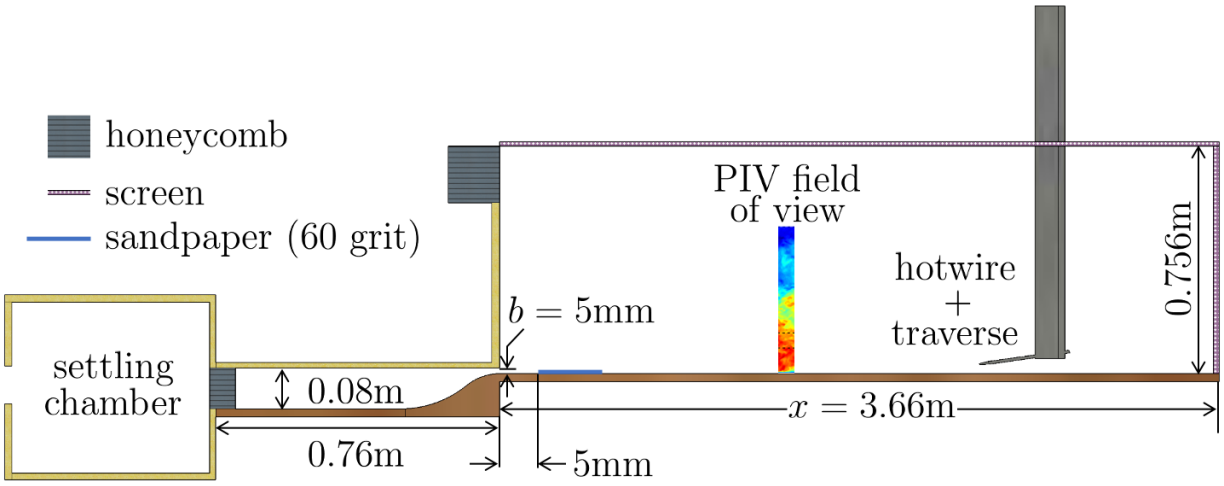

Figure 2: A Schematic showing the salient features of the experimental set up.

as much as possible, the influence of the forcing on the inner wall layer transition. Most measurements were carried out at a nominal jet Reynolds number $Re_j = bV_j/\nu \approx 5960$, where V_j is nominal PWJ exit centerline velocity and ν the kinematic viscosity. A speaker produced the forcing in the plenum chamber. A range of forcing Strouhal numbers were consider spanning $St = f_f b/V_j \approx 0.28 - 5.7 \times 10^{-3}$. Here, f_f was the forcing frequency. All perturbations considered were large-perturbations to the base flow as with respect to the outer scales the perturbation were such that $U_m/f_f > 1.6\delta$.

Hot-wire anemometry (HWA) based measurements were carried out at several streamwise locations spanning $x/b = 1$ to $x/b = 162$. The hot-wire sensors were boundary-layer type probes with a diameter d =2.5 µm at a nominal aspect ratio of $l/d = 200$. Complementary time-resolved particle image velocimetry (PIV) measurements were also carried out. These measurements were centered at a nominal downstream location of $x/b = 137$. These measurements resulted in a single wall-normal slice of temporally resolved measurements. Hence, these measurements are comparable to an array of synchronous, multi-component hot-wire measurements. The wall-normal mean velocity $\overline{w}$ in a PWJ is non-zero therefore, HWA based measurements measure an effective velocity U. On the other hand PIV based mea-

surements measures both components of the velocity i.e., the streamwise and wall-normal velocities (u and w respectively). The wall-normal ordinate is z and the streamwise ordinate is x.

The PIV based measurements were a mosaic of two cameras at different magnifications. One of the cameras focused on the inner boundary layer was at a higher magnification with a final interrogation window of $\Delta z^+ \times \Delta x^+ \approx 4 \times 4$. The top camera at a lower magnification had a final interrogation window of $\Delta z^+ \times \Delta x^+ \approx 6 \times 6$. The superscript $^+$ is indicative of normalization with respect to viscous or inner units. The friction velocity U_τ was measured using a curve fit process where the careful near wall measurements were carried out using HWA. For the rest of this report, the superscript 0 is used to identify unperturbed quantities while the superscript * is used to denote perturbed quantities. Also, the PWJ flow is broadly separated into an inner wall region which spans wall-normal locations less than the location of the maximum velocity i.e., $z < z_m$ (see schematic of figure 1)). The region above $z > z_m$ is the outer jet region of the PWJ.

3. Results & Discussion

A brief summary of the key observation and associated implications are presented here. First the effect of forcing Strouhal number is summarized. Following this the changes to the flow field while forcing at a single Strouhal number is presented in detail, to highlight exmplemary features of the forced flow.

Effect of Strouhal Number

A range of Strouhal numbers $St = f_f b/V_j = b/\lambda_j \approx 0.28 - 5.7 \times 10^{-3}$ were considered. Here, λ_j is the forcing wavelength based on the PWJ jet exit height b. The focus is specifically on changes to the wall shear stress τ_w or skin friction. The reduction in wall shear stress, is shown here as a reduction in friction velocity $U_\tau = \sqrt{\tau_w/\rho}$. This is shown as a function

of forcing Strouhal number as well as streamwise location in figure 3. A reduction in the wall-shear stress was observed for all excitation wavelengths, as well as for all streamwise distances considered. It is seen that for all the streamwise distances considered there is a specific wavelength ($\approx 3.3 \times 10^{-3} b/\lambda_j$, $\lambda_j = V_j/bf_f$) at which a clear maximum reduction in friction velocity U_τ is obtained. This wavelength is independent of downstream distance though the actual % reduction in U_τ is a function of downstream distance. The maximum reduction in U_τ was at a downstream distance of $x/b = 100$ after which the reduction decreases for all downstream distances considered.

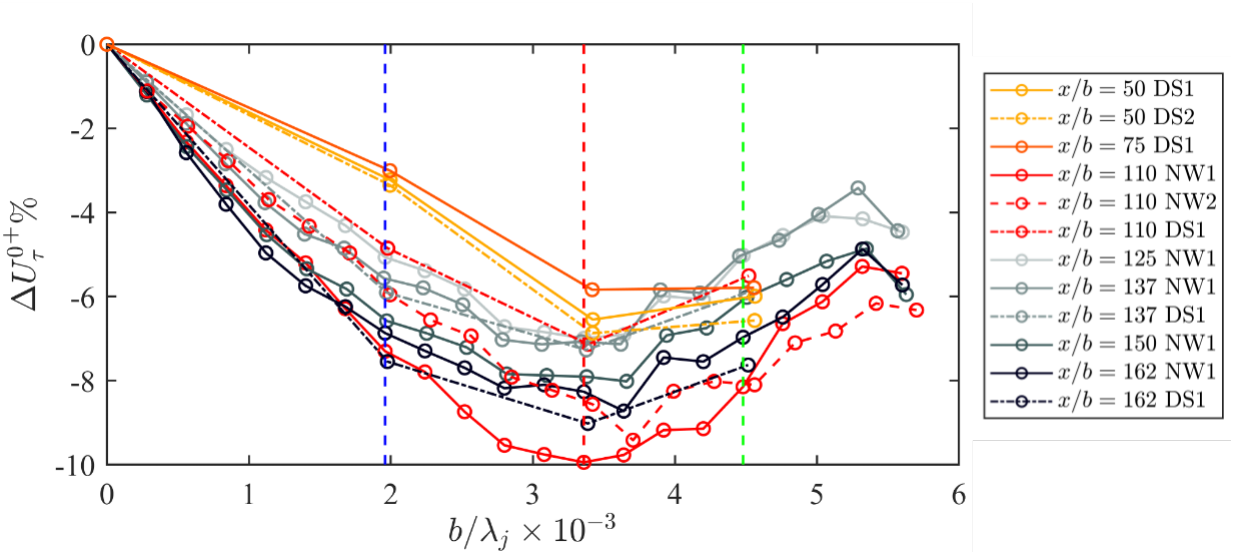

Figure 3: The reduction in friction velocity ΔU_τ as a function of the Strouhal number $St = b/\lambda_j$ at various streamwise locations. The vertical dashed lines show the forcing frequencies $f_f = 7$ Hz (- - -), $f_f = 12$ Hz (- - -) and $f_f = 16$ Hz (- - -) respectively. Detailed results from $f_f = 7$ Hz is presented in this report.

Results presented in this report are primarily from forcing at $f_f = 7$ Hz (blue line in figure 3). This case is referred to here on as case A. The internal mechanisms of the PWJ at this forcing was representative of the behavior at other forcing frequencies. At this forcing frequency $f_f = 7$ Hz, the perturbation wavelength was $\lambda_{xf} \approx 6.6\delta$ (based on the outer

scales at the downstream location $x/b = 137$). In this case, the perturbation increased the turbulence intensity at the PWJ exit centerline from $< 1\%$ to 5.5%, making it a large-amplitude forcing. Other forcing frequencies $f_f = 12$ (referred to as case B) and 16 Hz (referred to as case C) where also studied in detail and are briefly presented here and in greater detail in the publications and dissertations funded by this work.

Mean Flow Statistics

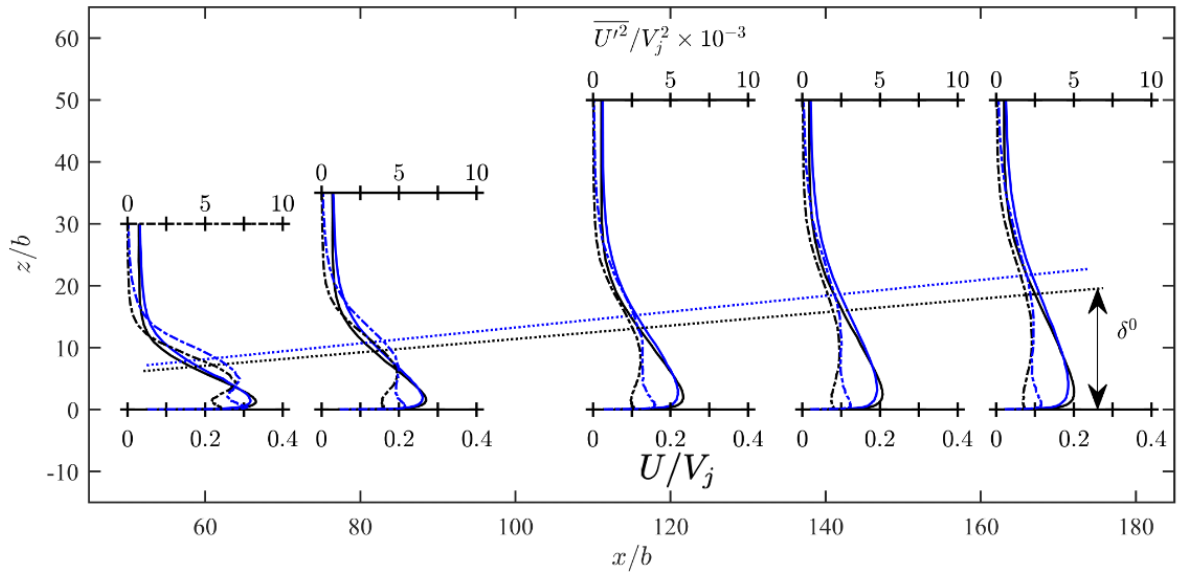

Figure 4: The solid lines show the mean effective streamwise velocity profile U as measured by HWA as the flow develops downstream of the PWJ exit. The dot-dashed line shows the corresponding evolution of the effective streamwise turbulence intensity $\overline{U'^2}$ profiles. The black lines are those corresponding to the unperturbed PWJ while the blue ones are those corresponding to the perturbed PWJ (case A). The development of the outer length scale δ is also shown indicating the spreading rate of the PWJ.

The streamwise evolution of the mean velocity as well as the turbulence intensity as measured by HWA is shown in figure 4. The mean velocity at $x/b = 137$ comparing the three different

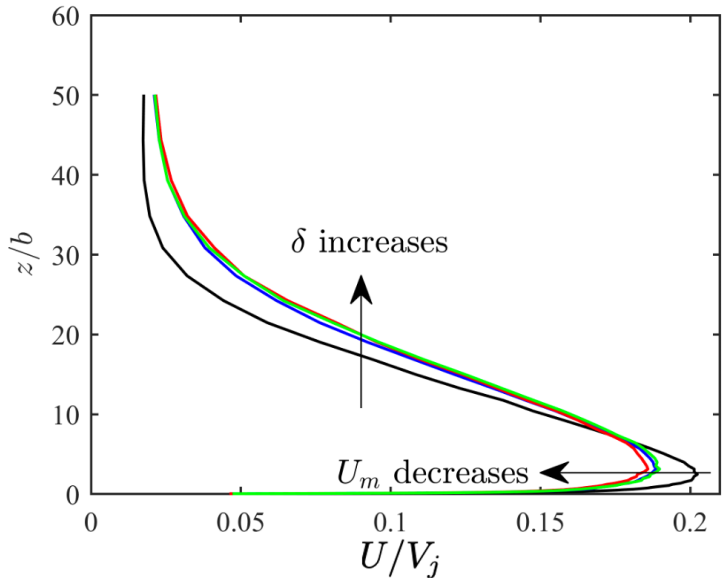

Figure 5: Mean velocity profiles at $x/b = 137$ for the unforced flow (—) and the forced flow; case A (—), case B (—) and case C (—).

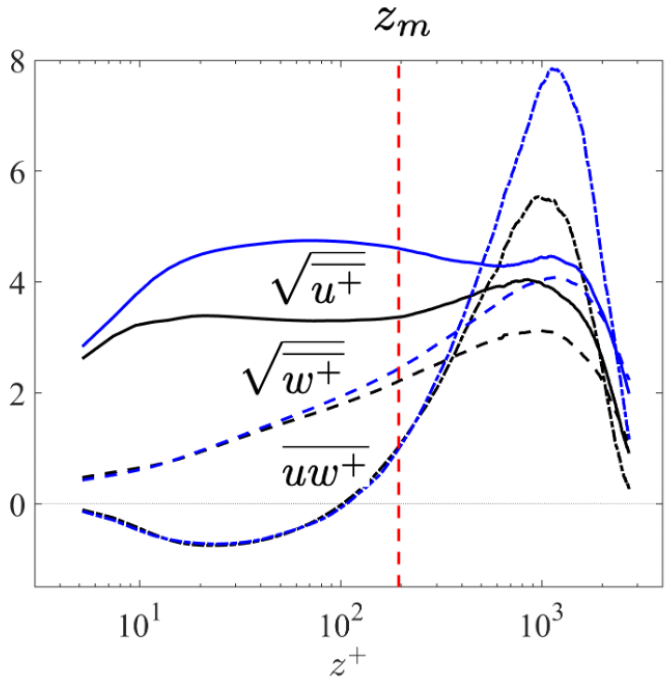

Figure 6: Turbulent stresses at $x/b = 137$ from PIV measurements for the unforced (black lines) and the case A forced flow (blue lines).

forcing highlighted in figure 3 is also shown. The maximum velocity, the outer velocity scale, U_m is reduced when the PWJ is forced. The outer length scale δ or the shear layer thickness on the other hand increases upon forcing. These large-scale changes together along with the decrease in U_τ increases the local Reynolds number $Re_\tau = u_\tau \delta/\nu$ when forced.

The turbulence intensity of the unforced PWJ has two peaks one in the inner wall region and the other in outer jet region. This is seen in figure 6 which shows the PIV based turbulence intensity at $x/b = 137$. The streamwise turbulence intensity in the inner wall region is increased considerably by the forcing. There is a smaller increase in the outer jet region. On the other hand there is little change in the spanwise turbulence intensity in the wall region, with a gradual increase moving outwards reaching a maximum increase in the jet region, coinciding with the location of the outer peak of the unforced flow. Similarly, the Reynolds shear stress shows virtually no change in the inner wall region but has an increase with a maximum increase around the outer peak. The streamwise evolution of the turbulence intensity as measured by HWA is shown also in figure 4. The behavior at $x/b = 137$, is shown to be typical of all other streamwise locations considered.

Skin friction and momentum

The variation of the skin friction coefficient $C_{f_j} = 2U_\tau^2/V_j^2$ as a function of downstream distance is shown in figure 7. The profiles for all three forcing cases are shown. C_{f_j} is seen to decrease upon forcing for all three cases consistent with figure 3, the maximum decreases at all streamwise locations being that corresponding to case B.

The forcing caused changes in the momentum residing in the inner and outer parts of the flow. The momentum in the flow is divided into two parts using a broad division based on wall normal location. The momentum in the flow in the inner wall region ($z < z_m$) and the outer region ($z > z_m$) is shown in figure 8 as function of downstream distance. The overall momentum in the flow is increased by the forcing at all streamwise locations. On the other

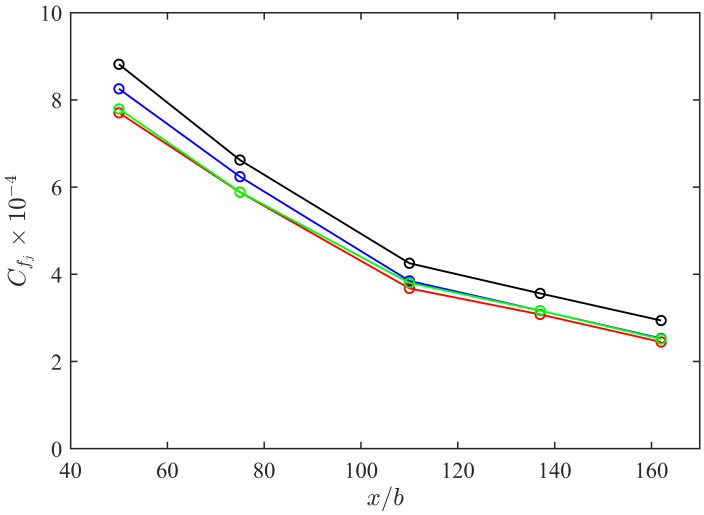

Figure 7: Skin friction coefficient $C_{f_j} = 2U_\tau^2/V_j^2$ as a function of streamwise distance x/b for the forced flow. The color convention from figure 5 is followed here.

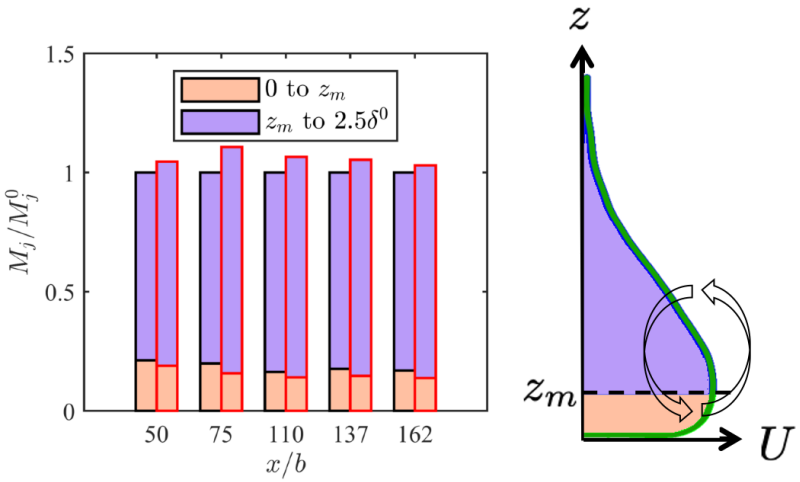

Figure 8: Flow momentum in the inner ($z < z_m$) and outer ($z > z_m$) regions of the flow. The variation is shown as a function of streamwise distance for case A. A schematic highlighting the enhanced mixing in the forced flow is also shown.

hand, the momentum in the inner wall region is reduced at all streamwise locations. The increased mixing in the flow upon forcing simultaneously removes high momentum fluid from the wall region while bringing in low momentum fluid from the outer region (see schematic of figure 8). This decreases the momentum in the wall region which the reduces the mean

skin friction coefficient.

Linear Response

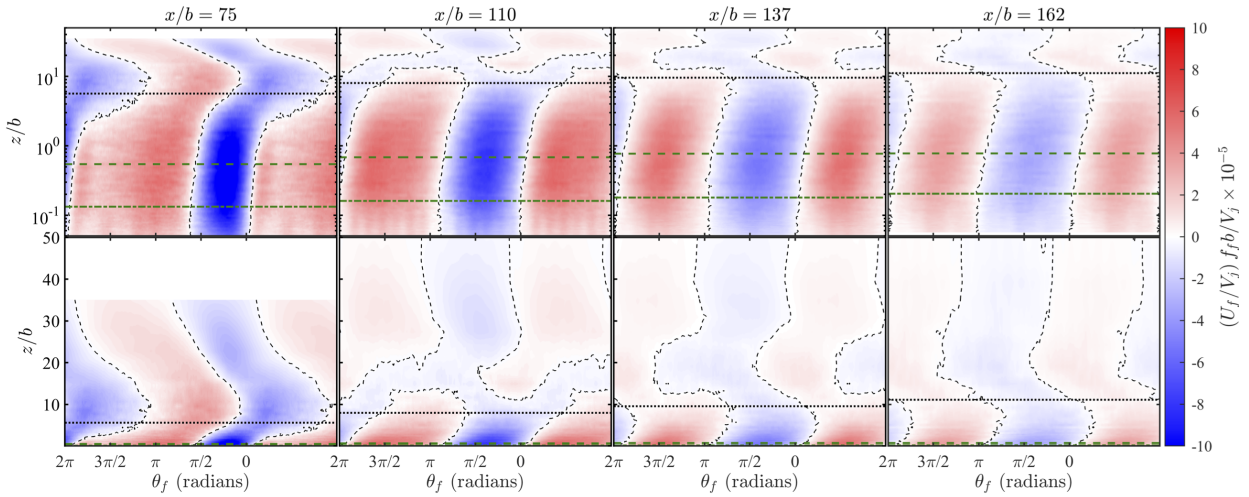

Figure 9: Variation of the linear response mode U_f in logarithmic coordinates (top) and linear coordinates (bottom) for case A. The red regions indicate positive fluctuation whereas the blue regions indicate negative fluctuations. The line (·····) is that corresponding to $U_f = 0$.

The linear response mode of the PWJ, due to the applied perturbation $U_f(\theta_f, z)$, as a function of downstream distance, is shown for case A in figure 9. These response modes were constructed based on phase-locked HWA measurements. At all streamwise locations the response in the wall region is a forward leaning flow structure. This structures is similar to the naturally occurring forward leaning structures observed in canonical boundary layers [32]. Such structures have also been observed to naturally occur in the wall region of the PWJ [33]. In the outer free-shear region, the linear response mode shows a structure that is backward leaning. Such backward leaning flow structures have also been naturally observed in the outer region of the PWJ [33]. At the most downstream locations where $x/b > 110$ the linear response modes appears to show a third structure in the outer reaches of the flow. These linear response modes observed in the forced flow at various wall-normal locations show a relative phase shift between each other as a function of streamwise distance. This indicates

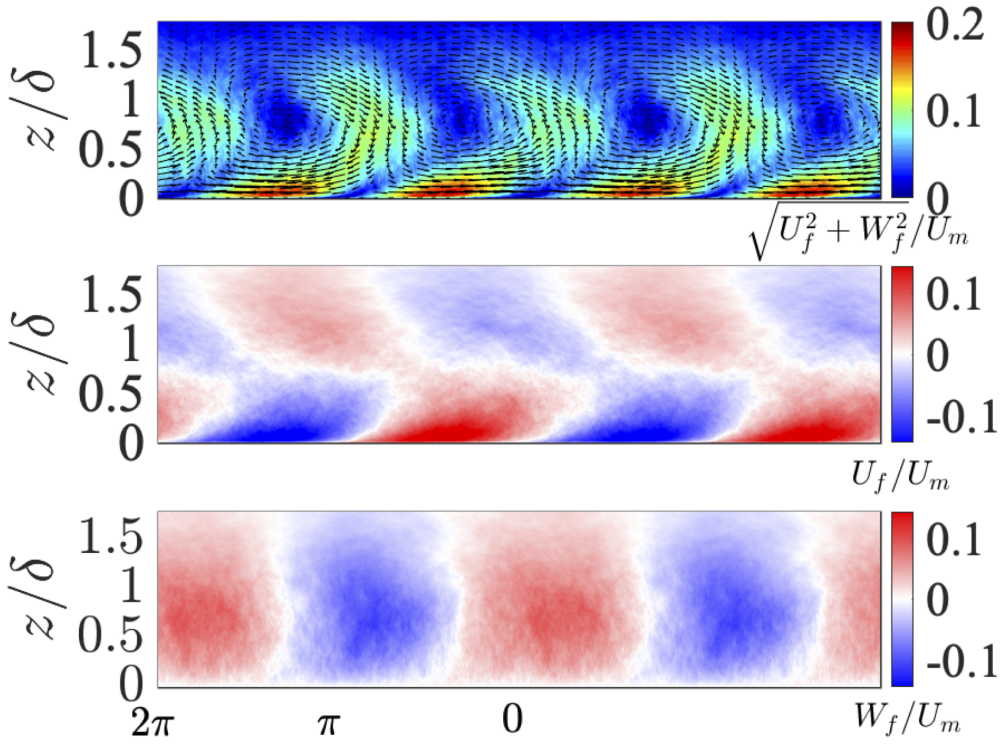

Figure 10: Linear response mode from the PIV based measurements. Both the streamwise U_f (middle) and wall-normal W_f (bottom) component are shown. The velocity vectors corresponding to these modes are also shown (top).

that these structures are convecting with different convection velocities.

The linear response mode from the PIV based measurements for case A at $x/b = 137$ is shown in figure 10. In this case, both the streamwise U_f and the wall-normal W_f modes are shown along with a vectorial representation of the modes. It is reiterated that the structure in the near-wall region is a forward leaning boundary layer like structure while the outer structure is a back leaning jet like structure. They are together associated with alternating regions of positive and negative wall-normal motions.

Spectral Response

First, the one-dimensional pre-multiplied energy spectra $f\phi_{uu}$ of the unforced flow is considered to highlight key flow features. Figure. 11 shows the spectra $f\phi_{uu}$ of the unforced flow

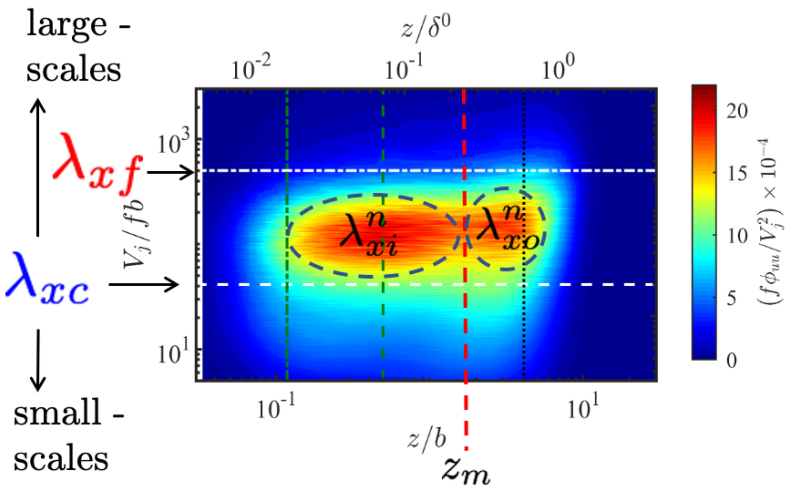

Figure 11: Contours of the pre-multiplied one-dimensional energy spectra $f\phi_{uu}$ at $x/b = 50$ for the unforced flow. λ_{xf} is the forcing wavelength, λ_{xc} is the cut-off wavelength that separates the large-scales from the small-scales. λ^n_{xi} are the naturally occuring energetic large-scales in the wall (inner) region and λ^n_{xo} are the naturally occuring energetic large-scales in the jet (outer) region. The wall-normal locations highlighted are $z^+ \approx 15$ (-·-·), $z^+ \approx 60$ (- - -) and $z \approx 0.6\delta^0$ (·····)

at $x/b = 50$. The energy spectra is presented as a function of a wavelength $V_j f/b$ and wall-normal distance z, where f are the Fourier frequencies. Shown also is the cut-off wavelength λ_{xc} that is used to separate the large-scales from the small-scales. Here, large-scales refers to those flow scales that are larger than twice the outer length scale of the unforced flow i.e., $\lambda_x > 2\delta^0$. The profiles of the spectra $f\phi_{uu}$ at three wall-normal locations ($z^+ \approx 15,\ 60$ and $z \approx 0.6\delta^0$) are shown in figure 12. These locations are chosen to represent the very-near wall region, a location in the log region and one in the outer jet region respectively. Much of the energy in the unforced PWJ resides in the large-scales of the flow. There are however two wall-normal locations where this energy is concentrated. One lies in the inner wall region centered around the wall-normal location $z^+ \approx 60$ and the other is in the outer jet region centered around the wall-normal location $z \approx 0.6\delta^0$. These energetic large-scale wavelengths are referred to as λ^n_{xi} and λ^n_{xo} respectively. Here, the superscript n is used to highlight that these are naturally occurring. Each of these group of energetic large-scale wavelengths λ^n_{xi}

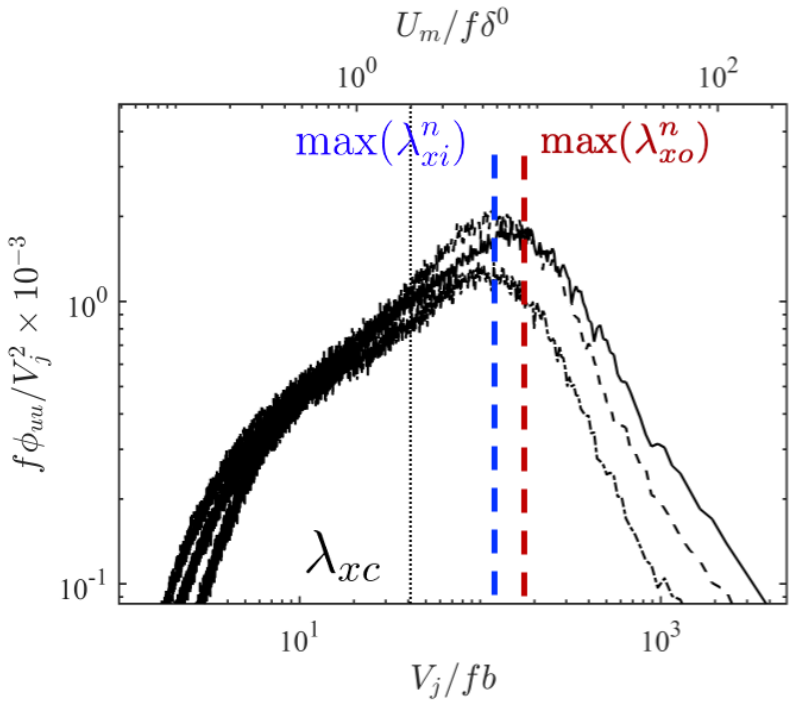

Figure 12: Profiles of the pre-multiplied one-dimensional energy spectra $f\phi_{uu}$ at $x/b = 50$ for the unforced flow showing the wall-normal locations highlighted in figure 11. The line styles are as follows, $z^+ \approx 15$ (-·-·), $z^+ \approx 60$ (- - -) and $z \approx 0.6\delta^0$ (—). Also highlighted are the cutoff wavelength λ_{xc} and the most energetic wavelengths in the wall region $\max(\lambda^n_{xi})$ and the outer region $\max(\lambda^n_{xo})$ respectively.

and λ^n_{xo} have a wavelength with maximum or peak energy and is referred to as $\max(\lambda^n_{xi})$ or $\max(\lambda^n_{xo})$ respectively. It is also noted that $\max(\lambda^n_{xi}) < \max(\lambda^n_{xo})$ (see figure 12).

The streamwise evolution of the energy spectra $f\phi_{uu}$ of the unforced flow and the forced flow is shown in figure 13. The forced flow spectra shown is that corresponding to case A. As the unforced flow develops downstream the energetic large-scales of the flow become larger with increasing downstream location i.e., λ^n_{xi} and λ^n_{xo} increase with x/b. However, the forcing wavelength λ_{xf} is fixed. Therefore, at the most upstream locations ($x/b \leq 110$) $\lambda_{xf} > \lambda^n_{xo} > \lambda^n_{xi}$. At a downstream location of $x/b \approx 110 - 137$, $\lambda_{xf} \approx \max(\lambda^n_{xo})$. At further downstream locations $\lambda_{xf} < \lambda^n_{xi} < \lambda^n_{xo}$.

Considering the forced spectra it is shown that the excess energy is always transferred

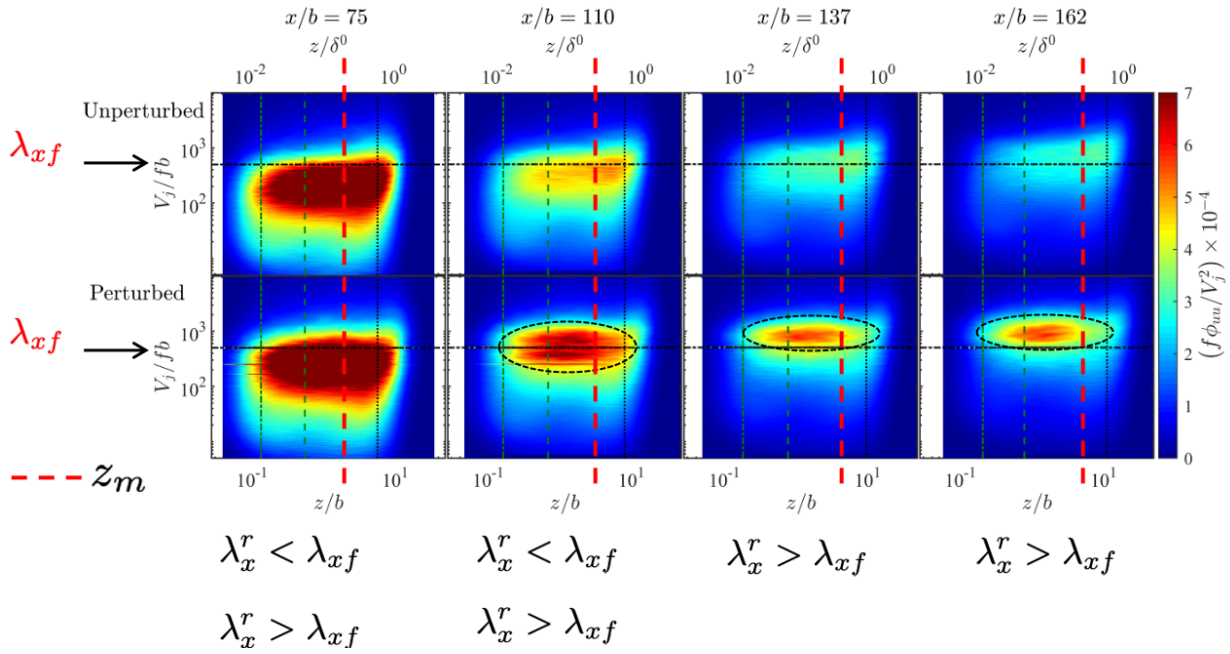

Figure 13: Streamwise evolution of the contours of the energy spectra $f\phi_{uu}$ for the unforced (top) and forced (bottom) flow (case A). The forcing scale λ_{xf} is also shown. The relative size of the forcing scale λ_{xf} to the recipient scales λ_x^r are indicated below the plots. The recipient scales λ_x^r in the forced spectra are highlighted over the contours (- - -).

to the inner wall region, the region that is occupied by the scales λ_{xi}^n. This is highlighted in the difference plot of figure 14, where the difference in spectra of the forced and unforced flow are shown as a function of streamwise distance. However, the recipient wavelengths λ_x^r of the excess perturbation energy are such that $\max(\lambda_x^r) \approx \max(\lambda_{xo}^n)$. In other words, the perturbation energy is transferred to a fixed set of scales $\lambda_{xr} \approx \lambda_{xo}^n$ at a fixed wall-normal location, the wall region. This is further highlighted in the line plots of figure 15. Here the profiles of the pre-multiplied energy spectra of the forced flow (case A) in the wall region ($z^+ \approx 15$ and 60) are compared with that of the unforced flow at $z \approx 0.6\delta^0$. For clarity, these profiles at $x/b = 162$ are shown in figure 16. These figure show that the wavelength corresponding to the most energetic recipient scales align with those of the naturally occurring structures in the outer jet region i.e., $\max(\lambda_x^r \approx \max(\lambda_{xo}^r)$.

Figure 13 and 14 also shows the relative size of the recipient scales λ_x^r and the forcing

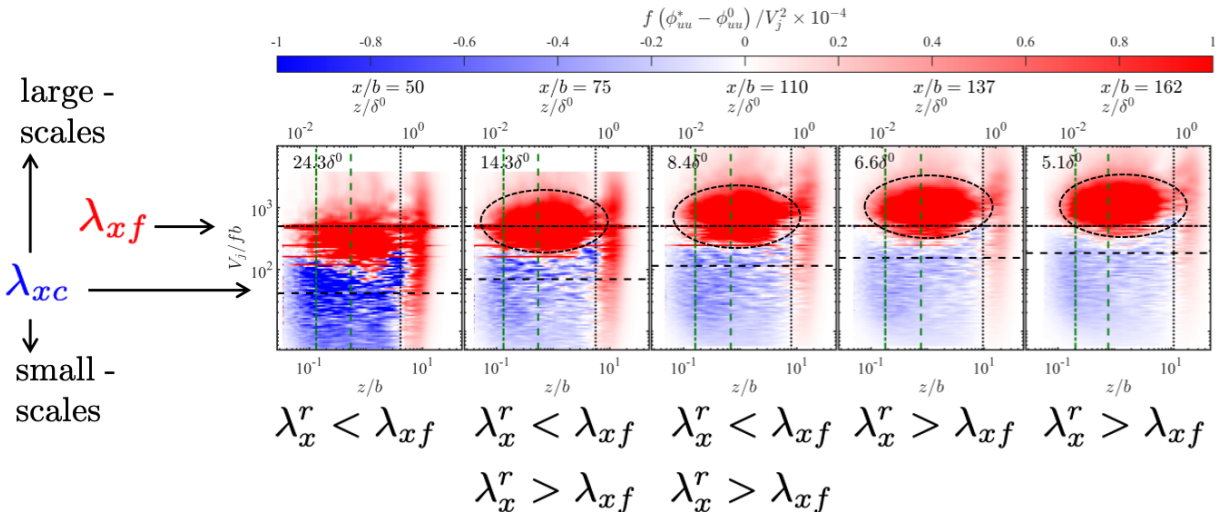

Figure 14: Streamwise evolution of the contours of the difference in the energy spectra $f(\phi^*_{uu}-\phi_{uu})$ between the forced (case A) and the unforced flow. The forcing scale λ_{xf} as well as the cutoff wavelength λ_{xc} are also shown. The relative size of the forcing scale λ_{xf} to the recipient scales λ^r_x are indicated below the plots. The recipient scales λ^r_x in the forced spectra are highlighted over the contours (- - -). The wall-normal locations highlighted are $z^+\approx15$ (-·-·-), $z^+\approx60$ (- - -) and $z\approx0.6\delta^0$ (·····)

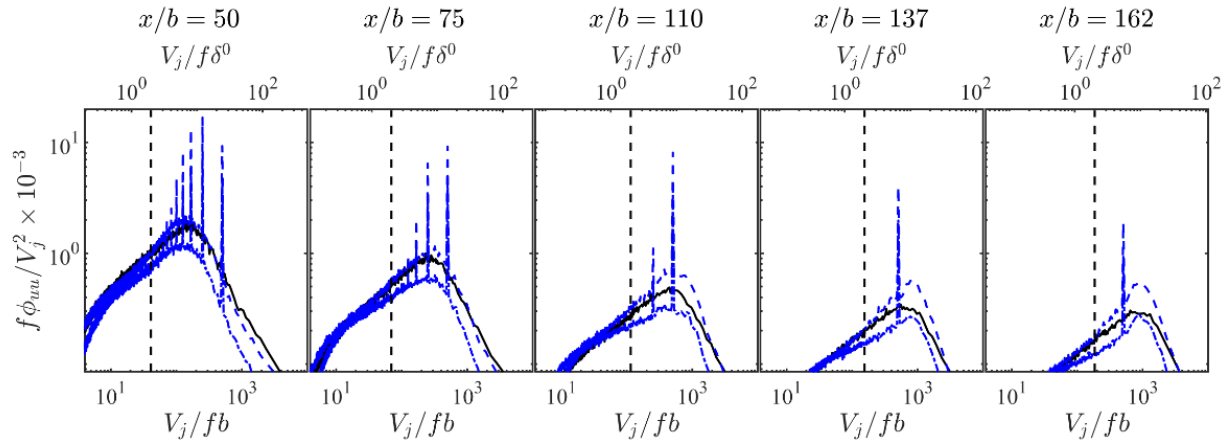

Figure 15: Compares the profiles of the pre-multiplied energy spectra of the forced flow (case A) at the wall-normal locations $z^+\approx60$ (-·-·-) and $z^+\approx60$ (- - -). Also shown is the profile of the spectra of the unforced flow at $z\approx0.6\delta^0$. These profiles are shown at various streamwise locations.

scale λ^f_x. At the upstream locations when $\lambda^r_x<\lambda_{xf}$ the direction of energy transfer is in the manner of a forward cascade while at the downstream locations when $\lambda^r_x>\lambda_{xf}$ the energy

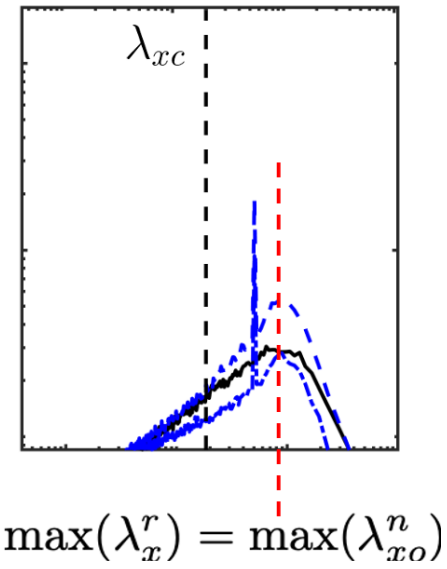

Figure 16: Compares the profiles of the pre-multiplied energy spectra at $x/b = 162$ of the forced flow (case A) at the wall-normal locations $z^+ \approx 60$ (-·-·-) and $z^+ \approx 60$ (- - -). Also shown is the profile of the spectra of the unforced flow at $z \approx 0.6\delta^0$.

transfer is in the manner of an inverse cascade. Figure 14 also shows that the energy in the small scales are consistently reduced everywhere in the wall region. However, in the far extremities of the flow $z > 0.6\delta^0$, there is an increase in the small scale energy.

Figure 17 shows the difference in the spectra between that at a given streamwise location and the immediately preceding streamwise location. This is shown for both the forced and unforced flow. This difference plot gives an estimate of the relative energy transfer between scales as the flow develops downstream. The scales that are loosing energy and the scales that are receiving energy as the unforced PWJ develops downstream are exactly the same as the ones that are receiving or loosing energy in the forced PWJ. This of course is except at the forcing frequency and its harmonics in the case of the forced PWJ. This suggests that the mechanisms that exist in the unforced flow are identical to those in the forced flow. Or stated differently, the forcing scale mimics the naturally occurring large-scale structures in the PWJ that occur at the forcing wavelength.

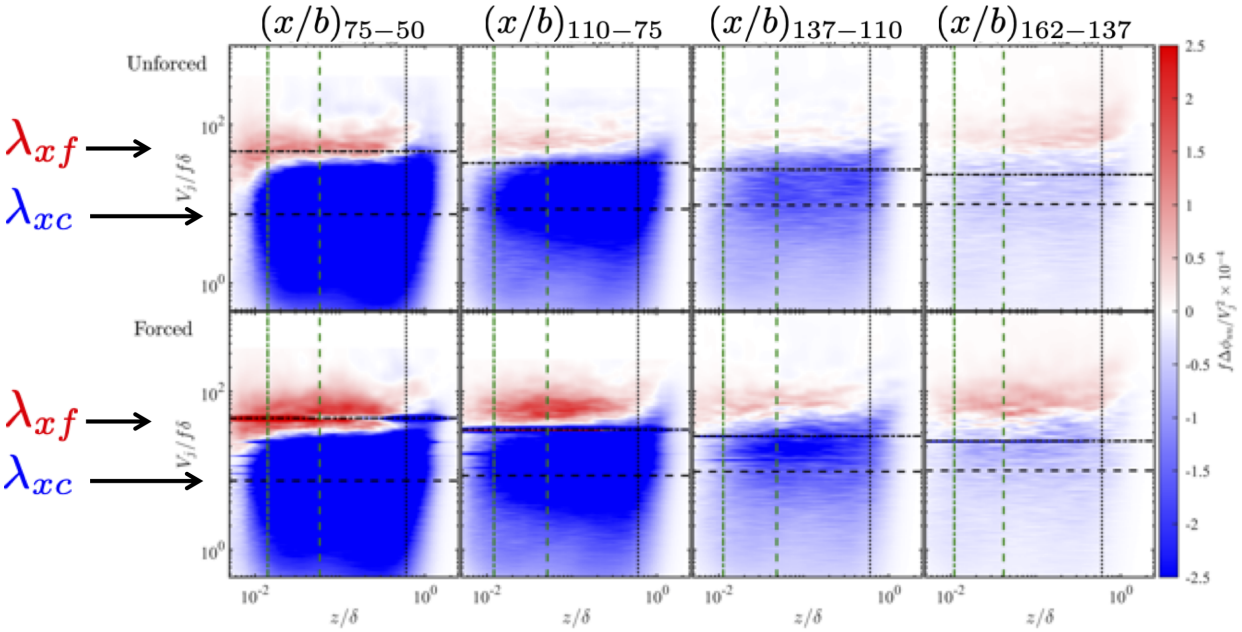

Figure 17: Streamwise evolution of the contours of the difference in the energy spectra $f\Delta\phi_{uu}$ between a given streamwise location and the immediately preceding streamwise location. This is shown for both the unforced (top) and the forced (bottom) flow (case A). The forcing scale λ_{xf} as well as the cutoff wavelength λ_{xc} are also shown. The wall-normal locations highlighted are $z^+ \approx 15$ (-·-·-), $z^+ \approx 60$ (- - -) and $z \approx 0.6\delta^0$ (·····)

This behavior is true for all cases (A, B and C) studied in depth. Figure 18 shows the profiles of the pre-multiplied energy spectra for the unforced and forced flow (cases A, B and C). The profiles are shown at three wall-normal locations, two in the inner wall region at $z^+ \approx 15$ and 60 and the other in the outer jet region at $z \approx 0.6\delta^0$. For all the cases the recipient wavelengths λ_x^r have a peak energy which occurs at approximately the same wavelength i.e., $\max(\lambda_x^r)$ is identical for all cases. In other words for all the scales of forcing considered, energy from the linear response modes in the near-wall region is being transferred to the outer jet scales. But this energy transfer occurs in the wall region. Also seen is that the small-scale energy for all the forcing scales considered is reduced in the wall region. The linear response mode also persists for longer streamwise distances in the wall region than in the outer region.

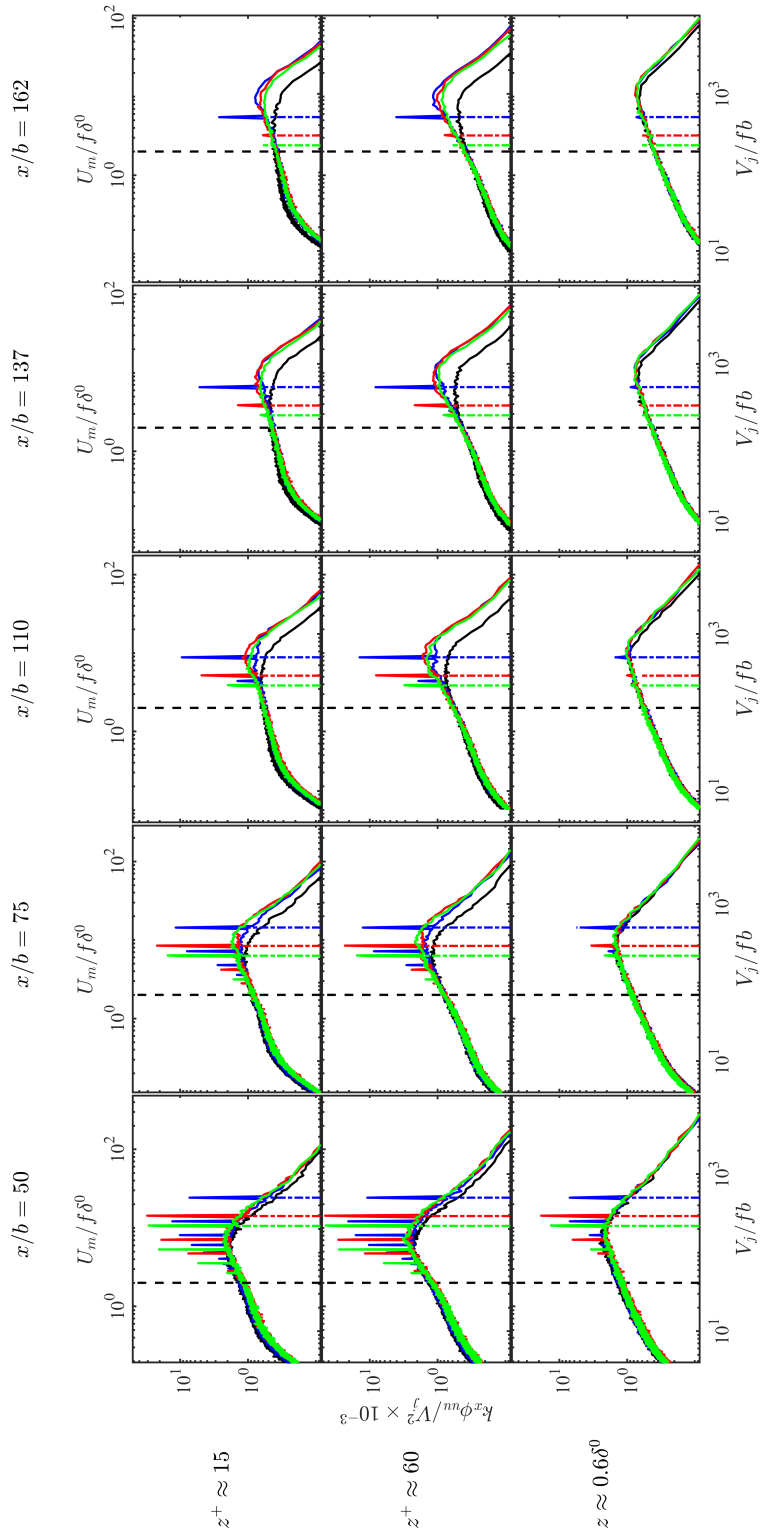

Figure 18: Profiles of the pre-multiplied energy spectra for the unforced (——) and forced flow; case A (——), case B (——) and case C (——). The profiles are shown at three wall-normal locations $z^+ \approx 15$ (top), $z^+ \approx 60$ (middle) and $z \approx 0.6\delta^0$ (bottom). The forcing scales for the three cases are also shown (dash-dot lines) as well as the cut off wavelength λ_{xc} (- - -).

Scale Interactions

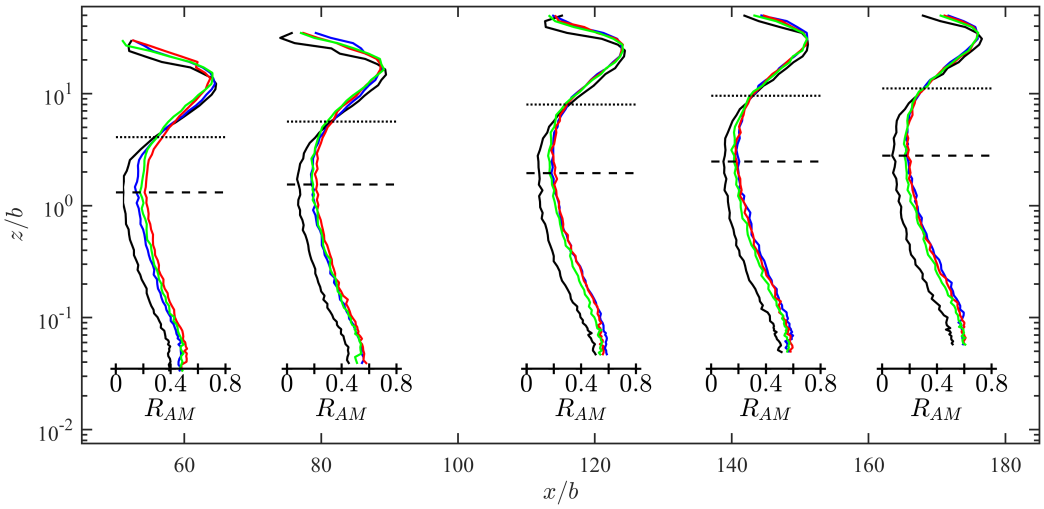

Figure 19: The variation of the profiles of the amplitude modulation coefficient R_{aM} as a function of streamwise distance. This is shown for both the unforced flow and the forced flow; case A (—), case B (—) and case C (—). Here, R_{AM} was derived from single wire HWA based measrurements.

The amplitude and frequency modulation caused by the large-scales were quantified using an amplitude and frequency modulation coefficient. The amplitude modulation coefficient R_{AM} as defined by Mathis et al. [1] was used when considering the single HWA measurements. The wavelet based approach of Baars et al. [16] was also used to calculate an amplitude R_{AM} and frequency modulation R_{FM} coefficient derived from PIV measurements. The HWA based R_{AM} is shown in figure 19. The profiles of R_{AM} for both the forced (case A, B and C) and the unforced flow are shown as the flow develops downstream. In the case of the unforced PWJ the amplitude modulation is highest in the near-wall region and then decreases towards the central region of the flow. It then increases again in the outer jet portion. In the case of the forced flows there is an increase in the modulation in the wall region while in the outer jet region there is not a substantial difference. This single-wire HWA based R_{AM} does not unambiguously capture inner-outer interactions as noted by Schlatter and Orlu [34].

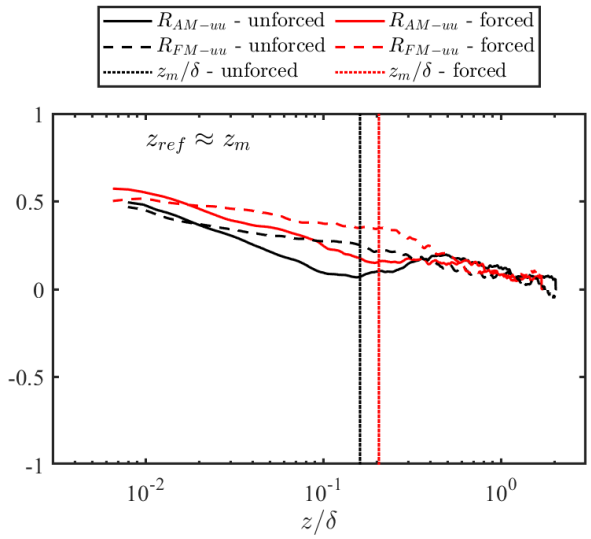

Figure 20: Profiles of the amplitude R_{AM-uu} and frequency R_{FM-uu} modulation coefficient for the unforced (black lines) and forced (case B, red lines) flow derived from PIV based measurements. This shows the modulation effect of the large-scales at $z_{ref} \approx z_m$ (dotted lines) on the finer streamwise scales across the flow.

However, the amplitude and frequency modulation coefficient R_{AM} and R_{FM} using the wavelet approach can quantify this interaction unambiguously. The streamwise large-scale at $z_{ref} \approx z_m$ is chosen as the reference large-scale u_L. The profiles of R_{AM} and R_{FM} with respect to this large-scale is shown in figure 20 and figure 21. Figure 20 captures the modulation of the finer streamwise scales (R_{AM-uu} and R_{FM-uw}) while figure 21 captures the modulation of the finer wall-normal scales (R_{AM-uw} and R_{FM-uw}). These are shown for both the forced flow (case B) and the unforced flow.

Considering the unforced flow, both R_{AM-uu} and R_{FM-uw} are highest in the very-near-wall region. This indicates that u_L has a large modulating effect on the streamwise smaller scales in this region. The modulating effect gradually decreases as the distance from the wall increases. In the jet region, moving outwards from z_m, R_{AM-uu} increases slightly and then decreases again. R_{FM-uu} on the other hand gradually decreases from a maximum in the wall region moving outwards into the jet region. When forced the coupling between scales

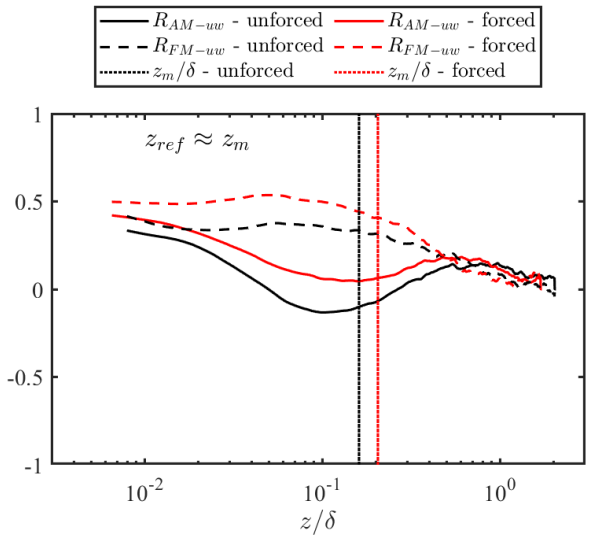

Figure 21: Profiles of the amplitude R_{AM-uw} and frequency R_{FM-uw} modulation coefficient for the unforced (black lines) and forced (case B, red lines) flow derived from PIV based measurements. This shows the modulation effect of the large-scales at $z_{ref} \approx z_m$ (dotted lines) on the finer streamwise scales across the flow.

in the wall region is increased as indicated by an increase in R_{AM-uu} as well as R_{FM-uu} in this region. There is no perceptible change upon forcing in the outer jet region.

The profiles of R_{AM-uw} and R_{FM-uw} are shown in figure 21. R_{AM-uw} like R_{AM-uu} is a maximum in the wall region for the unforced flow, indicating significant coupling between the scales. Away from the wall, R_{AM-uw} decreases and then becomes negative in the region around $z/\delta = 0.1$. Moving outwards from the wall R_{AM-uw} increases to become positive and then decreases slightly at the PWJ outer edge. When $z/\delta < 0.1$, R_{FM-uw} is maximum, positive and nearly a constant. R_{FM-uw} while remaining positive gradually decreases into the jet region. When forced R_{AM-uu} and R_{FM-uu} both increase in the wall region with no perceptible change in the outer region. Together these observations emphasize that the large-scale, large-perturbation forcing considered altered the internal interactions of the flow, particularly the inner-outer interactions.

Effect of Co-Flow

To study the effect of a co-flow on the PWJ a co-flow experimental setup was also built. A schematic highlighting the various salient features of the co-flow PWJ is shown in figure 22. In this case the forcing was only applied to the co-flow portion of the flow. The co-flow velocity was V_c.

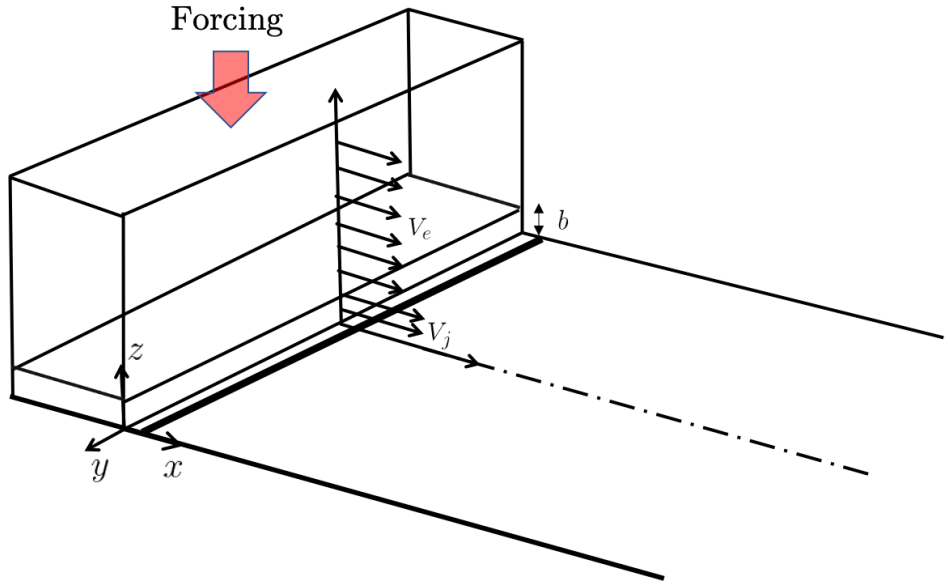

Figure 22: Schematic of the PWJ with co-flow showing salient features.

The preliminary mean velocity profiles of the co-flow PWJ in the case of a forced and unforced case is shown in figure 23. Here, the forcing shown was at 5 Hz, which is again a large-scale forcing to the flow. The ratio of the co-flow to the PWJ velocity was $V_j/V_c \approx 1.5$. The mean velocity as measured by HWA is shown at three different streamwise locations ($x/b = 60, 100$ and 150). The flow is seen approaching a flat-plate boundary layer like state at the most downstream location. There are no substantial changes to the co-flow upon forcing. The corresponding turbulence intensities is presented in figure 24. In the outer extremities of the flow (the co-flow region) there are significant changes to the turbulence intensities, the region directly subject to the forcing. However, particularly as the flow develops downstream

subtle increases in the turbulence intensity are observed in the wall region. This is showed in the figure 25 where the region around the near-wall peak of figure 24 is shown. The forcing has consistently increased the overall near-wall turbulence intensity. This suggests that the effects of forcing only the co-flow has penetrated into the near-wall region.

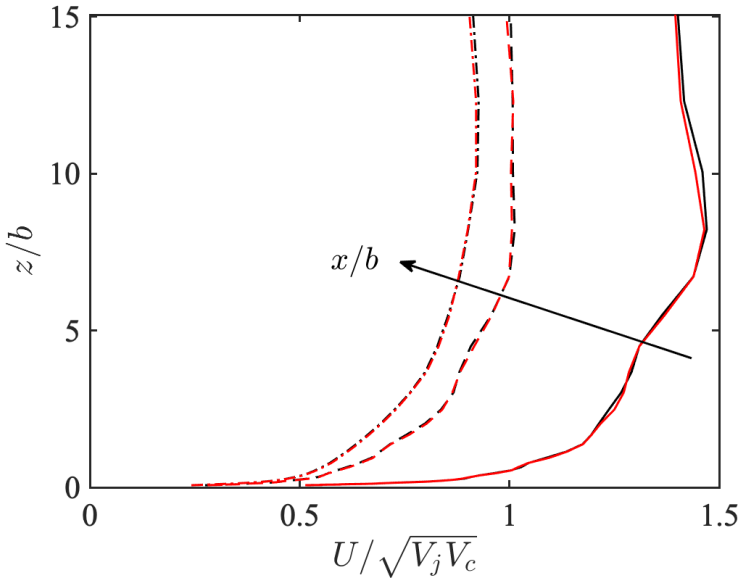

Figure 23: Variation of the mean velocity of the co-flow PWJ for both the forced (red lines) and the unforced (black lines) cases at various downstream locations ($x/b = 60, 100$ and 150).

Unsteady Jet

During the intial phase of the work it was proposed to use a use an unsteady or impulsive jet to control the PWJ during the later part of the work. The direction, with the agreement of the program manager, was then turned to focus on the PWJ with a co-flow motivated by the physics discovered in the jet without a co-flow. The usteady jet lead to a conference presentations and a publication which were partially supported by this work, the key findings of which are briefly summarized here.

The unsteady flows produced by consecutively pulsed, transient jets were studied using

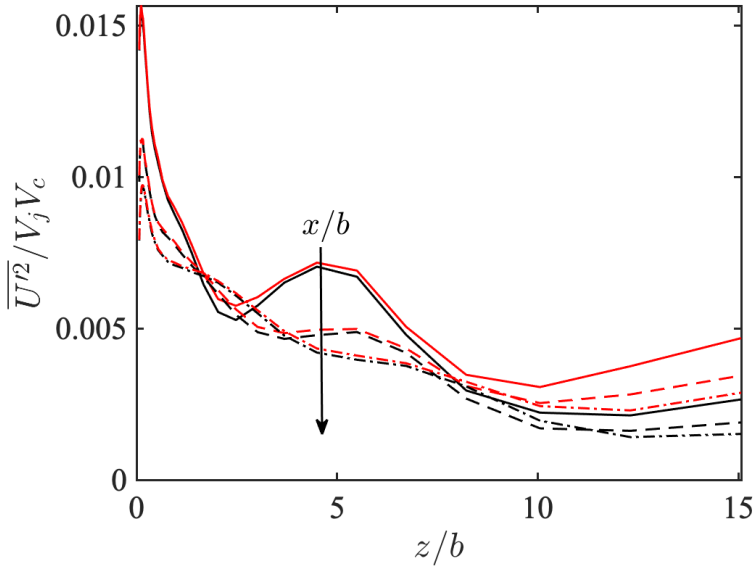

Figure 24: Variation of the turbulence intensity of the co-flow PWJ for both the forced (red lines) and the unforced (black lines) cases at various downstream locations ($x/b = 60, 100$ and 150).

HWA and PIV. A typical flow visualization from a single pulse of momentum is shown in figure 26. Two successive volumes of fluid were ejected from a jet nozzle into a quiescent fluid. The time between these two consecutive pulse were varied. The Reynolds number based on the nozzle diameter was 1500. The interactions between the two volume of fluids changed significantly based on the separation between the events. When the time interval was short the starting vortex for the second volume of fluid was not completely formed. The momentum flux increase due to the first ejection of fluid stabilized the near flow field of the second ejection, thereby eleminating the starting vortex. This also reduced the entrainment caused by the starting vortex. This work then showed that fron a flow control perspective, when an unsteady jet is used as an actuator, the time scale introduced by the jet unsteadiness needs to be taken into account while considering its effectiveness.

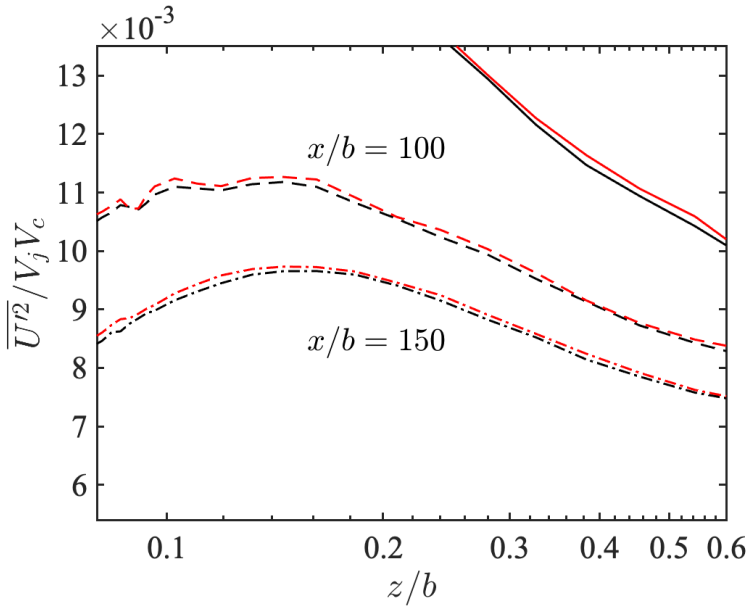

Figure 25: Variation of the turbulence intensity of the co-flow PWJ for both the forced (red lines) and the unforced (black lines) cases at various downstream locations ($x/b = 60, 100$ and 150). This figure shows a zoomed in view of the region around the near-wall peak of the intensties shown in figure 25.

Figure 26: Flow visualization of an unsteady jet with a single pulse of momentum

4. Summary

Key conclusions and its implications are summarized here as follows:

1. A plane wall jet was subject to large-scale, large-perturbation forcing over a range of Strouhal numbers. All forcing Strouhal numbers lead to a reduction in friction velocity with reductions up to $\approx$10% being observed.

2. There was no substantial change to the shape of the mean velocity profile upon forcing. However, the outer length scale increased while the outer velocity scale decreased.

3. The reduction in friction velocity upon forcing was accompanied by a reduction in momentum in the wall region of the flow. This was due to the large-scale mixing caused by the forcing.

4. There was no substantial change in the wall-normal turbulence intensity and the Reynolds shear stress, in the wall region, when the flow was forced. However, there was a substantial increase in the streamwise turbulence intensity in the wall region. All stress components showed an increase in the outer jet region.

5. The linear response modes resulted in flow structures that mimicked the naturally occurring flow structures in the respective flow regions. The jet region mode was backward leaning while the wall region structures were forward leaning.

6. The excess energy from forcing was transferred primarily to flow scales that matched the wavelength of the naturally occurring outer jet structures. However, this transfer occurred in the wall region. This transfer of energy was in the manner of a forward cascade at upstream location and in the manner of an inverse cascade at downstream locations.

7. The preceding observation lead to the conclusion that the natural energy transfer pathway within the PWJ was to transfer energy from the wall layer structures to the outer jet like structures. The forcing hence, highlighted an energy transfer pathway in the flow where the input energy was at the forcing frequency.

8. The forcing also increased the coupling between the large-scales and finer scales of the flow. Both the amplitude and frequency modulation of the finer scales in the wall region was enhanced by the forcing.

9. These observations has implications for modelling as well as controlling these flows. First, as the linear response mode mimics the naturally occurring large-scale flow structures in the respective flow regions it supports the viewpoint that the linear dynamics of the Navier-Stokes equation dictates the nature of the large-structures in the flow. The non-linearities of the flow then only serve to transfer energy between flow scales. However, this transfer is not trivial as it was highlighted that this can be both in the manner of a forward as well as inverse cascade.

10. The increased inner-outer interactions and the reduced friction velocity point to changes in the near-wall cycle caused by the large-scale forcing. Hence, it has been experimentally shown that large-scale inputs can be used to effecetively control the near-wall region of complex wall-bounded flows such as the PWJ.

5. Publications, Talks, Conferences & Dissertations

Journal articles

Accepted:

1. Gnanamanickam E. P., Bhatt S., Artham S. K. & Zhang Z., "Large-Scale Motions in a Plane Wall Jet", *Journal of Fluid Mechanics*, Vol. 877, pp. 239–281, DOI.

2. Zhang Z., Seth D., Artham S., Leishman J. G., & Gnanamanickam E. P., "Time-Resolved Flow Field Measurements of Momentum Driven Pulsed, Transient Jets", *AIAA Journal*, Vol. 56, No. 4, pp. 1434–1446, 2018, DOI.

In process:

3. Bhatt S., & Gnanamanickam E. P., "Linear and Non-Linear Mechanisms Within a Forced Plane Wall Jet", (under review).

4. Gnanamanickam E. P., Artham S. K. & Zhang Z., "Inner-Outer Interactions in a Forced Plane Wall Jet", (under final preparation, to be submitted Apr 2020).

It is anticipated at least one other journal publication, to be submitted in 2020, will be funded by this grant.

Invited talks

1. Gnanamanickam E.P., "Energy Transfer Pathways in Non-Canonical Wall Turbulence", University of Central Florida, MAE Seminar Series, February 8, 2019.

2. Gnanamanickam E. P., Bhatt S.*, Artham S.*, & Zhang Z., "Turbulence Control by Targeting the Large-Scale Motions Within Boundary Layers", *FlowPAC Seminar*, University of Notre Dame, Mar. 2017.

Conferences and Proceedings

1. Artham S., Bhatt S., Zhang Z., & Gnanamanickam E. P., "Estimation of wall-shear stress and its variation in a unperturbed and perturbed plane wall-jet", *Bulletin of the American Physical Society*, Nov 2019.

2. Gnanamanickam, E. P., Bhatt S., Artham S., "Energy Transfer Within A Perturbed Plane Wall Jet", *11th International Symposium on Turbulence and Shear Flow Phenomena, 2019*, July-Aug 2019, Link.

3. Bhatt S., Artham S., & Gnanamanickam E. P., "Evidence of an Inverse Cascade in a Plane Wall Jet Through Large-Scale Forcing", *Bulletin of the American Physical Society*, Nov 2018.

4. Bhatt S., Artham S., & Gnanamanickam E. P., "Skin Friction Reduction Through Large-Scale Forcing", *Bulletin of the American Physical Society*, Nov 2017.

5. Zhang Z., Artham S., Leishman J. G., & Gnanamanickam E. P., "Time-Resolved Flow Field Measurements of Momentum Driven Pulsed, Transient Jets", *AIAA Science and Technology Forum and Exposition 2017: 55$^{\text{th}}$ Aerospace Sciences Meeting*, Grapevine, Texas, Jan 2017 (AIAA 2017-1890), DOI.

6. Artham S., Zhang Z., & Gnanamanickam E. P., "An Experimental Study of Momentum-Driven Unsteady Jets", *AIAA Science and Technology Forum and Exposition 2017: 55$^{\text{th}}$ Aerospace Sciences Meeting*, Grapevine, Texas, Jan 2017 (AIAA 2017-1889), DOI.

7. Bhatt S*., Artham S., & Gnanamanickam E. P., "The Effect of Excitation on the Plane Wall Jet", *Bulletin of the American Physical Society*, Nov 2016,.

Doctoral disserations

1. Bhatt, Shibani – "Flow interactions within a perturbed plane wall jet", May 2019.

2. Artham, Sravan Kumar – Topic: flow interactions within wall turbulence, expected Dec. 2020.

References Cited

[1] R. Mathis, N. Hutchins, and I. Marusic. Large-scale amplitude modulation of the small-scale structures in turbulent boundary layers. *Journal of Fluid Mechanics*, 628:311 – 37, 2009. doi: 10.1017/S0022112009006946.

[2] R. Mathis, J. P. Monty, N. Hutchins, and I. Marusic. Comparison of large-scale amplitude modulation in turbulent boundary layers, pipes, and channel flows. *Physics of Fluids*, 21(11):1 – 4, 2009. doi: 10.1063/1.3267726.

[3] I. Jacobi and B. J. McKeon. Phase relationships between large and small scales in the turbulent boundary layer. *Experiments in Fluids*, 54(3), 2013. doi: 10.1007/s00348-013-1481-y.

[4] A. J. Smits, B. J. McKeon, and I. Marusic. High-Reynolds number wall turbulence. *Annual Review of Fluid Mechanics*, 43:353 – 75, 2011. doi: 10.1146/annurev-fluid-122109-160753.

[5] I. Marusic, R. Mathis, and N. Hutchins. Predictive model for wall-bounded turbulent flow. *Science*, 329(5988):193–196, 2010. doi: 10.1126/science.1188765.

[6] I. Marusic, B. J. McKeon, P. A. Monkewitz, H. M. Nagib, A. J. Smits, and K. R. Sreenivasan. Wall-bounded turbulent flows at high Reynolds numbers: Recent advances and key issues. *Physics of Fluids*, 22:065103, 2010. doi: 10.1063/1.3453711.

[7] G. L. Brown and A. S. W. Thomas. Large structure in a turbulent boundary layer. *Physics of Fluids*, 20(10):S243–S252, 1977. doi: 10.1063/1.861737.

[8] P. R. Bandyopadhyay and A. K. M. F. Hussain. The coupling between scales in shear flows. *Physics of Fluids*, 27(9):2221 – 2228, 1984. doi: 0.1063/1.864901.

[9] D. Chung and B. J. McKeon. Large-eddy simulation of large-scale structures in long channel flow. *Journal of Fluid Mechanics*, 661:341 – 364, 2010. doi: 10.1017/S0022112010002995.

[10] M. Guala, M. Metzger, and B. J. McKeon. Interactions within the turbulent boundary layer at high reynolds number. *Journal of Fluid Mechanics*, 666:573 – 604, 2011. doi: 10.1017/S0022112010004544.

[11] M. Bernardini and S. Pirozzoli. Inner/outer layer interactions in turbulent boundary layers: A refined measure for the large-scale amplitude modulation mechanism. *Physics of Fluids*, 23(6):–, 2011. doi: 10.1063/1.3589345.

[12] B. Ganapathisubramani, N. Hutchins, J. P. Monty, D. Chung, and I. Marusic. Amplitude and frequency modulation in wall turbulence. *Journal of Fluid Mechanics*, 712:61 – 91, 2012. doi: 10.1017/jfm.2012.398.

[13] Z. Harun, J. P. Monty, R. Mathis, and I. Marusic. Pressure gradient effects on the large-scale structure of turbulent boundary layers. *Journal of Fluid Mechanics*, pages 477 – 498, 2013. doi: 10.1017/jfm.2012.531.

[14] L. Agostini and M. A. Leschziner. On the influence of outer large-scale structures on near-wall turbulence in channel flow. *Physics of Fluids*, 26(7):–, 2014. doi: 10.1063/1.4890745.

[15] K. M. Talluru, R. Baidya, N. Hutchins, and I. Marusic. Amplitude modulation of all three velocity components in turbulent boundary layers. *Journal of Fluid Mechanics*, 746, 5 2014. doi: 10.1017/jfm.2014.132.

[16] W. J. Baars, K. M. Talluru, N. Hutchins, and I. Marusic. Wavelet analysis of wall

turbulence to study large-scale modulation of small scales. *Experiments in Fluids*, 56 (10), 2015. doi: 10.1007/s00348-015-2058-8.

[17] B. E. Launder and W. Rodi. The turbulent wall jet. *Progress in Aerospace Sciences*, 19:81–128, 1981. doi: 10.1016/0376-0421(79)90002-2.

[18] B. E. Launder and W. Rodi. The turbulent wall jet measurements and modeling. *Annual Review of Fluid Mechanics*, 15(1):429–459, 1983. doi: 10.1146/annurev.fl.15.010183.002241.

[19] Y. Katz, E. Horev, and I. Wygnanski. The forced turbulent wall jet. *Journal of Fluid Mechanics*, 242:577 – 609, 1992. doi: 10.1017/S0022112092002507.

[20] M. D. Zhou, C. Heine, and I. Wygnanski. The effects of excitation on the coherent and random motion in a plane wall jet. *Journal of Fluid Mechanics*, 310:1 – 37, 1996. doi: 10.1017/S0022112096001711.

[21] M. Schober and H.-H. Femholz. Turbulence control in wall jets. *European Journal of Mechanics, B/Fluids*, 19(4):503 – 28, 2000. doi: 10.1016/S0997-7546(00)00131-X.

[22] D. Ahlman, G. Brethouwer, and A. V. Johansson. Direct numerical simulation of a plane turbulent wall-jet including scalar mixing. *Physics of Fluids*, 19(6), 2007. doi: 10.1063/1.2732460.

[23] Z. Pouransari, G. Brethouwer, and A. V. Johansson. Direct numerical simulation of an isothermal reacting turbulent wall-jet. *Physics of Fluids*, 23(8):085104, 2011. doi: 10.1063/1.3622774.

[24] Z. Pouransari, L. Vervisch, and A. V. Johansson. Heat release effects on mixing scales of non-premixed turbulent wall-jets: A direct numerical simulation study. *International*

Journal of Heat and Fluid Flow, 40(0):65 – 80, 2013. doi: 10.1016/j.ijheatfluidflow.2012.12.005.

[25] A. Dejoan and M. A. Leschziner. Large eddy simulation of a plane turbulent wall jet. *Physics of Fluids*, 17(2):1 – 16, 2005. doi: 10.1063/1.1833413.

[26] R. K. Agarwal and W. Bower. Navier-stokes computations of turbulent compressible two-dimensional impinging jet flowfields. *AIAA Journal*, 20(5):577–584, 1982. doi: 10.2514/3.51113.

[27] M. K. Looney and J. J. Walsh. Mean-flow and turbulent characteristics of free and impinging jet flows. *Journal of Fluid Mechanics*, 147:397–429, 10 1984. ISSN 1469-7645. doi: 10.1017/S0022112084002147.

[28] K. Jambunathan, E. Lai, M. A. Moss, and B. L. Button. A review of heat transfer data for single circular jet impingement. *International Journal of Heat and Fluid Flow*, 13 (2):106 – 115, 1992. ISSN 0142-727X. doi: 10.1016/0142-727X(92)90017-4.

[29] J. Rauleder and J. G. Leishman. Particle–fluid interactions in rotor–generated vortex flows. *Experiments in Fluids*, 55(3):1–15, 2014. doi: 10.1007/s00348-014-1689-5.

[30] J. Rauleder and J. G. Leishman. Flow environment and organized turbulence structures near a plane below a rotor. *AIAA Journal*, 52(1):146 – 161, 2014. doi: 10.2514/1.J052315.

[31] I. Wygnanski, Y. Katz, and E. Horev. On the applicability of various scaling laws to the turbulent wall jet. *Journal of Fluid Mechanics*, 234:669 – 90, 1992. doi: 10.1017/S002211209200096X.

[32] M. Tutkun, W. K. George, J. Delville, M. Stanislas, P. B. V. Johansson, J.-M. Foucaut,

and S. Coudert. Two-point correlations in high reynolds number flat plate turbulent boundary layers. *J. Turb.*, 10:N21, 2009. doi: 10.1080/14685240902878045.

[33] R. Banyassady and U. Piomelli. Turbulent plane wall jets over smooth and rough surfaces. *Journal of Turbulence*, 15(3):186–207, 2014. doi: 10.1080/14685248.2014.888492.

[34] P. Schlatter and R. Orlu. Quantifying the interaction between large and small scales in wall-bounded turbulent flows: A note of caution. *Physics of Fluids*, 22(5):1 – 4, 2010. doi: 10.1063/1.3432488.